

1 **DOI: <https://doi.org/10.47391/JPMA.31245>**

2 **A novel feature-agnostic approach for glaucoma detection in fundus**  
3 **images**

4  
5 **Nadia Rasool<sup>1</sup>, Zulkaif Sajjad<sup>2</sup>, Furqan Shaukat<sup>3</sup>, Syeda Filzah Bukhari<sup>4</sup>,**  
6 **Mahmood Ali<sup>5</sup>, Farah Akhtar<sup>6</sup>**

7 **1,4-6** Department of Glaucoma, Al-Shifa Trust Eye Hospital, Rawalpindi, Pakistan.

8 **2,3** Department of Electrical, University of Engineering and Technology, Taxila, Pakistan.

9 **Correspondence:** Nadia Rasool. **Email:** [nadiafrqn@gmail.com](mailto:nadiafrqn@gmail.com)

10 **ORCID ID:** 0009-0008-1383-2283

11  
12 **Abstract**

13 **Objective:** To design and validate a fully automated, feature-agnostic deep learning  
14 approach for the early detection of glaucoma from fundus images.

15 **Method:** The retrospective study was conducted at Al-Shifa Trust Eye Hospital,  
16 Rawalpindi, Pakistan, using publicly available retinal fundus image datasets from  
17 October 2024 to January 2025 and comprised 1,707 fundus images from five  
18 publicly available retrospective datasets.

19 A computer-aided detection system was employed based on state-of-the-art deep  
20 convolutional neural networks, including EfficientNetV2b0, Xception, InceptionV3,  
21 Visual Geometry Group and ResNet50. The images were labelled either as  
22 glaucomatous or healthy after they were pre-processed through cropping,  
23 normalisation and data augmentation. The models were fine-tuned using transfer  
24 learning, and evaluated using standard metrics, such as accuracy, precision, recall,  
25 F1-score and area under the curve, which were calculated using Python-based  
26 statistical libraries.

27 **Results:** Among the tested models, EfficientNetV2b0 achieved the best  
28 performance with an area under the curve of 0.98 and an accuracy of 93%. The

29 best-performing model achieved a sensitivity/recall of 97%, precision of 89% and  
30 F1-score of 93%, indicating reliable performance for glaucoma classification. The  
31 robustness of the proposed method was validated across multiple datasets, ensuring  
32 its generalisability in diverse clinical scenarios.

33 **Conclusion:** The proposed deep learning-based approach provided a reliable and  
34 efficient method for early glaucoma detection. Its automation and high accuracy  
35 made it suitable for use in mass screening programmes and under-resourced clinical  
36 environments, potentially reducing the burden on ophthalmologists and enabling  
37 timely intervention.

38 **Key Words:** Glaucoma detection, Fundus imaging, Computer-aided diagnosis, Optic  
39 nerve head, optical disc, Optical cup.

40

## 41 **Introduction**

42 Glaucoma is a chronic and irreversible disorder of the optic nerve (ON) and remains  
43 one of the primary causes of total blindness across the globe [1]. It is widely  
44 recognised as a major public health concern, impacting millions of individuals  
45 worldwide. Reports indicate that over 70 million people were living with glaucoma in  
46 2020, and projections suggest this figure may increase to nearly 112 million by 2040  
47 [2,3]. The disease progresses gradually and, without timely diagnosis and  
48 management, can result in permanent ON damage and eventual loss of vision.  
49 Pathologically, glaucoma is characterised by structural alterations within the ON head  
50 (ONH), particularly thinning of the retinal nerve fibre layer [4]. These changes are  
51 often associated with impaired blood supply and increased intraocular pressure (IOP),  
52 affecting ON. The optic disc (OD), a distinct yellowish circular region of the retina,  
53 serves as the point where numerous retinal nerve fibres gather and transmit visual  
54 information from the eye to the brain.

55 Computer-aided diagnosis (CAD) has increasingly reshaped modern healthcare, with  
56 notable impact in ophthalmology. By integrating machine learning (ML) and deep  
57 learning (DL) techniques with high-resolution ocular imaging, CAD tools assist

58 clinicians in identifying diseases, such as glaucoma, more reliably [5]. These systems  
59 support timely clinical decisions, facilitate early treatment, and ultimately contribute  
60 to improved patient outcomes. As the technology advances, it holds strong potential  
61 for delivering more precise and widely accessible screening solutions for eye  
62 disorders. Fundus imaging plays a central role in these applications, as it enables  
63 visualisation of retinal structures, detection of pathological changes, and monitoring of  
64 disease progression. Through detailed retinal analysis, ophthalmologists gain  
65 meaningful insights into structural alterations associated with ocular conditions. In  
66 addition, CAD-supported screening programmes enhance efficiency, reduce costs, and  
67 expand access to eye-care services — particularly in resource-limited settings [4].  
68 Fundus photography, a non-invasive technique using a dedicated retinal camera,  
69 captures clear images of OD, the optic cup (OC), and surrounding retinal features,  
70 thereby supporting early glaucoma detection and follow-up assessment.  
71 Initially, efforts were made to examine retinal images using traditional image  
72 processing techniques. However, these strategies were limited and confined by their  
73 reliance on hand-crafted features, and inability to generalise across varied patient  
74 populations.  
75 Glaucoma arises mainly due to the loss of ON fibres and astrocytes. In glaucoma, the  
76 size of the neural rim and OC decreases with respect to OD. Several studies have  
77 primarily focused on this loss, examining it by using fundus images. Cheng et al. [6]  
78 proposed a method based on Cup-to-Disc Ratio (CDR) to examine glaucoma. They  
79 used a superpixel classification technique to segment the OC and OD. After  
80 segmentation, they calculated the CDR for glaucoma assessment. Likewise, Saha et  
81 al. [7] calculated the CDR after segmenting the OC and OD using level-set  
82 techniques. They used 6671 images for the test from seven publicly available  
83 datasets, and the system achieved an accuracy of 97.4%. A method proposed by  
84 Amed et al. [8] involves first detecting the OD using brightness and template  
85 matching techniques. It then calculates the CDR using the segmented OC and OD for  
86 classifying the healthy and glaucoma-affected eye images. For this purpose, the

87 authors utilised the DRISHT-GS (a retinal fundus image dataset for optic nerve head  
88 segmentation and glaucoma screening/assessment) [9] dataset and achieved good  
89 results compared to other CDR feature-based approaches.

90 Yin et al. [10] proposed the combined method of novel optimal channel selection and  
91 knowledge-based circular Hough transform for segmenting the OC and OD. They  
92 used 324 fundus images to evaluate and achieve the average dice coefficient for OC  
93 and OD, which was 0.81 and 0.92, respectively, with a CDR error of 0.10.

94 The study by Cheng et al. [11] used a super pixel classification method to calculate  
95 the CDR for predicted masks of the OD and OC as part of glaucoma screening. This  
96 method evaluated 650 fundus images, resulting in average overlapping errors of  
97 9.5% for OD and 24.1% for OC. The method achieved area under the curve (AUC)  
98 values of 0.820 and 0.800 in two separate databases.

99 Chan et al. [12] proposed an approach that combined and utilised the patient's  
100 personal data and genomic information along with fundus images to achieve an AUC  
101 of 0.866 for glaucoma detection. This method outperformed individual components  
102 0.551 for personal data, 0.722 for images, and 0.810 for genomic information.  
103 However, a limitation of this method is its reliance on handcrafted features created  
104 by expert human graders. For this reason, new algorithms perform better and rely on  
105 automatic feature extraction methods.

106 Early advancements in medical image analysis utilise advanced ML and DL methods  
107 to improve disease diagnosis. Convolutional neural networks (CNNs) are frequently  
108 used in the assessment of glaucoma due to their robustness and strong generalisability  
109 across various cross-domain datasets. CNNs are replacing classic algorithms in the  
110 examination of diseases [13]- [14].

111 Chan et al. [15] proposed a six-layer CNN model for glaucoma diagnosis. This model  
112 consists of four convolutional layers and two fully connected layers. They trained the  
113 network from scratch and evaluated it using the Online Retinal Fundus Image  
114 Database for Glaucoma Analysis and Research (ORIGA) and Singapore Chinese Eye  
115 Study (SCES) private datasets. The ORIGA dataset contains 650 images, including

116 482 healthy cases and 168 glaucomatous cases. In contrast, the SCES dataset  
117 comprises 1,676 images, with only 46 of them being glaucomatous. The results  
118 indicated an AUC of 83.1% and 88.7% in the two databases. The main disadvantage  
119 was class imbalance, and another limitation of this work was the challenge in  
120 reproducing the results, as the SCES and ORIGA datasets are private and not publicly  
121 available.

122 In the work conducted by Alghamdi et al. [16], a combined CNN approach was  
123 utilised to detect OD abnormalities. The first architecture was designed to identify the  
124 OD region, while the second CNN model classified the OD into three categories:  
125 abnormal, normal and suspicious. For this study, the authors used four publicly  
126 available datasets: DIARETDB1 (Standard Diabetic Retinopathy Database Calibration  
127 Level 1), STARE (Structured Analysis of the Retina), DRIVE (Digital Retinal Images  
128 for Vessel Extraction), and MESSIDOR (Methods to Evaluate Segmentation and  
129 Indexing Techniques in the Field of Retinal Ophthalmology). A limitation of this  
130 research was that these datasets were not specifically intended for glaucoma  
131 classification, as they were created for different purposes. This means that it is  
132 uncertain whether or not the images contained glaucoma cases.

133 Orlando et al. [17] proposed a method that utilised two pre-trained CNNs for  
134 glaucoma screening: the Visual Geometry Group (VGG-16) and the OverFeat. They  
135 were used to generate feature vectors from fundus images. Before training, the authors  
136 pre-processed the images by cropping around the ONH and applying contrast-limited  
137 adaptive histogram equalisation. For evaluation, they used the DRISHTI-GSI dataset  
138 and reported average receiver operating characteristic (ROC) curve values of 0.76  
139 and 0.71. The main limitation of this work was the limited number of test images to  
140 evaluate the performance of these architectures.

141 Joshi et al. [18] proposed a method for OC segmentation that utilises anatomical  
142 evidence, specifically the bends of vessels at the cup's boundary. They localised the  
143 OD and OD based on vessel geometry and subsequently calculated CDR. Their  
144 evaluation was conducted on 138 fundus images, which included 105 from

145 glaucomatous patients and 33 from healthy individuals. The resulting error in the  
146 vertical cup-to-disc diameter ratio was  $0.09\pm 0.08$ , while the cup-to-disc area ratio  
147 error was  $0.12\pm 0.10$ .

148 As can be seen, most studies have focused heavily on CDR-based analysis, where  
149 performance strongly depends on how accurately the OC and OD are segmented, often  
150 using relatively small datasets. Although DL methods have improved automation and  
151 predictive capability, several works still face issues, such as class imbalance, limited  
152 generalisability, and a lack of reproducibility due to private datasets. These limitations  
153 suggest the need for more robust and clinically adaptable approaches to glaucoma  
154 detection.

155 The current study was planned to explore and evaluate the potential of five deep  
156 convolutional neural networks (DCNNs) to diagnose glaucoma from fundus images,  
157 and to develop a fully automatic and highly accurate method using state-of-the-art  
158 (SOTA) DL model for glaucoma detection using fundus images.

159

## 160 **Materials and Methods**

161 The retrospective study was conducted at Al-Shifa Trust Eye Hospital, Rawalpindi,  
162 Pakistan, using publicly available retinal fundus image datasets from October 2024  
163 to January 2025, and comprised 1,707 fundus images from five publicly available  
164 retrospective datasets. As this study used publicly available retrospective datasets,  
165 the exact image acquisition period was not consistently reported across all datasets.  
166 Therefore, the study period refers to the period during which the datasets were  
167 accessed, processed, and analyzed. A computer-aided detection system was  
168 employed based on SOTA DCNNs, including EfficientNetV2b0 (EfficientNet,  
169 Version 2, B0 variant), Xception, InceptionV3, VGG16 (Visual Geometry Group 16-  
170 layer network), and ResNet50. The study used five publicly available retrospective  
171 datasets: DRISHTI-GS [9], RIM-ONE [19], ACRIMA [20], SJCHOI86-HRF [21],  
172 and HRF (High-Resolution Fundus) [21]. Among these, ACRIMA [20] was the most  
173 suitable due to its large number of images. The sample size (1,707 fundus images)

174 was determined based on data availability from the five publicly accessible datasets  
175 [19-21]. Since all the datasets used were publicly available and fully anonymised, no  
176 written consent from the participants was required.

177 For dataset pre-processing, the images were first cropped around the ONH using the  
178 bounding box of 1.5 times the OD radius. Images in the RIM-ONE [19] dataset were  
179 initially cropped around the OD. The fundus images were cropped using a (290x290)  
180 and (224x224) window size around the identified centre [8], depending on the DCNN  
181 model's default input image size requirements. Additionally, Orlando et al. [19]  
182 showed that when applying CNN models for glaucoma assessment, cropping the  
183 images around the OD proved to be a more efficient method than using the complete  
184 fundus image. The dataset was divided into three parts for training, validation and  
185 testing of DL models: 80% for training, 10% for validation, and 10% for testing. To  
186 enhance accuracy and to achieve proper convergence, data augmentation techniques  
187 were applied. These techniques included random geometric transformations, such as  
188 rotations (rang: 0-30 degrees), shearing (rang: 0-20 degrees), and zooming (range: 0-  
189 20%) as well as both vertical and horizontal flips.

190 Fundus images with clear visibility of the OD and OS were included, and labelled as  
191 glaucomatous or healthy by clinical experts in the respective datasets.

192 Images with poor illumination, motion blur, missing labels, or artifacts that obstructed  
193 the ONH region were excluded.

194 For model development, five SOTA DCNNs were used: EfficientNetV2b0 [25],  
195 Xception [26], Inceptionv3 [27], VGG16 [28] and ResNet50 [29]. By leveraging  
196 transfer learning, the pre-trained ImageNet weights were fine-tuned for the specific  
197 task of glaucoma detection. Each model had distinct architectural advantages  
198 contributing to their effectiveness in screening for glaucoma disease.  
199 EfficientNetV2b0 [25], introduced by Tan and Le in 2021, utilises Fused Mobile  
200 Inverted Bottleneck Convolution (Fused-MBConv) layers that combine depth wise  
201 and pointwise convolutions into a single operation. The training speed improved by  
202 replacing the MBConv module with the Fused-MBConv module in the initial layers.

203 The architecture consists of six convolutional blocks; the first three blocks are Fused-  
204 MBConv layers, and the last three contain the MBConv layers. A non-uniform  
205 scaling strategy increases the number of deeper layers while achieving faster training  
206 times and improving efficiency compared to the previous versions of  
207 EfficientNetV2b0.

208 Xception [26], developed by Francois Chollet at Google, builds upon the Inception  
209 architecture by replacing the standard convolutions in the Inception modules with  
210 depth wise separable convolutions, significantly reducing the number of parameters  
211 compared to standard convolution layers. It consists of two main processes. In depth  
212 wise convolution, a single filter is applied to each input channel independently. This  
213 differs from the standard convolution operation, in which a filter is applied across  
214 all channels together. Depth wise convolution performs separate convolutions for  
215 each channel, which reduces the computational complexity of the operation. In  
216 pointwise convolution, a  $1 \times 1$  filter is applied across all channels to combine the  
217 results of the depth wise convolutions of different channels. This operation is also  
218 known as a channel-mixing convolution because it gets the information from  
219 different channels without affecting the spatial dimensions of the feature map.

220 InceptionV3 [27], introduced by Szegedy et al. [27] in ImageNet Large Scale Visual  
221 Recognition Challenge (ILSVRC) 2015, is an extension of GoogleNet. It consists of  
222 interconnected inception modules stacked together. Each module combines different  
223 types of convolutions to extract features from input images. InceptionV3 utilises  
224 multiscale and factorised convolutions to decrease the number of parameters while  
225 preserving complexity by breaking down large convolutions into smaller ones. It uses  
226 a combination of  $1 \times 1$ ,  $3 \times 3$  and  $5 \times 5$  convolution filters to extract features; the  $1 \times 1$   
227 convolutions are computed before  $3 \times 3$  and  $5 \times 5$  convolutions that reduce the  
228 dimensionality of the image. These modules address overfitting and computational  
229 expense by using dimensionality reduction through stacked  $1 \times 1$  convolutions. This  
230 approach reduces the number of parameters, resulting in a faster and more efficient  
231 network.

232 VGG16 [28], introduced by Simonyan and Zisserman [28] in 2014 at the ILSVRC  
233 (Figure 1), comprises 13 convolutional layers, five pooling layers, and three fully  
234 connected layers. It demonstrates remarkable performance in various computer vision  
235 applications. With its straightforward yet efficient sequential structure, VGG16 has  
236 become well-known among researchers. The model is widely used in research and is  
237 often considered a reference CNN for assessing performance on a wide range of tasks.  
238 ResNet50 [29], introduced by He et al [29], in 2015, is a 50-layer CNN that uses  
239 residual blocks with skip connections to address the vanishing gradient problem. It  
240 consists of 49 convolutional layers, a global average pooling layer, and a fully  
241 connected layer for classification. ResNet50 achieves high accuracy and  
242 computational efficiency through a bottleneck structure that includes 1x1 and 3x3  
243 convolutions.

244 In the current study, the models were fine-tuned using transfer learning and  
245 evaluated using standard metrics, such as accuracy, precision, recall, F1-score, and  
246 AUC [22], which were calculated using Python-based statistical libraries (scikit-  
247 learn [23] and NumPy [24]) through the following expressions:

$$248 \text{ Accuracy} = \frac{TP+TN}{TP+TN+FP+FN} \quad (1)$$

$$249 \text{ Precision} = \frac{TP}{TP+FP} \quad (2)$$

$$250 \text{ Recall} = \frac{TP}{TP+FN} \quad (3)$$

$$251 \text{ F1} = \frac{2 * \text{Precision} * \text{Recall}}{\text{Precision} + \text{Recall}} \quad (4)$$

252

## 253 **Results**

254 The combined datasets contained 1,707 fundus images; 919(53.8%) labelled as  
255 glaucoma and 788(46.2%) as healthy. For binary classification problems, the final  
256 predictions of the model would produce four results. One, true positive (TP) correctly  
257 predicting positive examples (correctly predicting results “Glaucoma”). Two, false  
258 positive (FP) incorrectly predicting positive examples (“Healthy” predicted results as

259 “Glaucoma”). Three, true negative (TN) correctly predicting results as “Healthy”. And,  
260 four, false negative (FN) incorrectly predicting “Glaucoma” as “Healthy”.

261 Standard performance metrics, namely accuracy, precision, recall, and f1-score,  
262 suggested that all models had strong diagnostic capability, with sensitivity and  
263 specificity values supporting their utility (Table).

264

## 265 **Discussion**

266 The ROC curve is commonly used to assess the discriminative ability of prediction  
267 models. It shows the overall performance of the model with a higher AUC, indicating  
268 better discrimination between classes.

269 The training procedure for fine-tuning the CNN models comprised effective fine-  
270 tuning, which involved leveraging the strengths of pre-trained models and customising  
271 them for glaucoma classification. The last fully connected layers were removed, and  
272 the Global Average Pooling (GAP) layer was added to reduce the spatial dimensions  
273 and retain useful features. The features were extracted from the GAP layer and then  
274 passed through the dense layer with 512 neurons, and Rectified Linear Unit (ReLU)  
275 activation was applied along with a Dropout layer with a rate of 0.5 to prevent  
276 overfitting. Subsequently, another dense layer with 256 neurons and ReLU activation  
277 was included, accompanied by a Dropout layer with a rate of 0.4. Finally, an output-  
278 dense layer with two neurons and a SoftMax activation function was added for binary  
279 classification. Adjustments were made that allowed the researchers to focus on the  
280 binary classification task, distinguishing between healthy and glaucomatous images.  
281 The models were trained on the publicly available datasets containing Healthy (H)  
282 and Glaucomatous (G) cases. For comparison analysis, five neural network  
283 architectures were trained: EfficientNetV2b0, InceptionV3, Xception, VGG16 and  
284 ResNet50. The study employed the Adam optimiser with a dynamic learning rate to  
285 train all the models, and binary cross-entropy was selected as the loss function for the  
286 binary classification task. The models were trained in batches of 120 epochs, with  
287 early stopping criteria based on validation loss to prevent overfitting. The performance

288 metrics were carefully monitored throughout the experimentation phase to identify the  
289 best-performing model for glaucoma detection.

290 These fine-tuned models were tested using ROC to determine the diagnostic validity  
291 of the glaucoma classifier across TP and FP rates. The area under the ROC curve  
292 (AUROC) is an essential parameter for evaluating classification performance since it  
293 measures the model's capacity to distinguish between healthy and glaucomatous  
294 classes successfully. Also, accuracy, precision, recall, and F1-score were calculated  
295 to measure the ability of each model to predict the retinal images effectively. Model  
296 evaluation was performed on the test set (10% of the total retinal images), which  
297 consisted of 174 retinal images, with 82 healthy images and 92 glaucomatous  
298 images. This was followed by two experiments. Firstly, each CNN model was fine-  
299 tuned to combine the dataset, which contained 1,707 retinal images, and to find the  
300 best CNN model, which was EfficientNetV2b0 (Table 1). In the second experiment,  
301 the best model was fine-tuned and tested on the ACRIMA dataset, as it was the  
302 largest dataset, containing 705 images. Examples of correctly classified retinal  
303 images, using the EfficientNetV2-B0 model, along with the prediction score on the  
304 ground-truth class, are shown in Figure 2.

305 Because the displayed curves closely resembled the top and left limits of the ROC  
306 space, they demonstrated the models' significant ability to detect glaucoma.

307 First, the outstanding capability of the DL models to differentiate between healthy  
308 and glaucomatous examples was demonstrated by AUROC values. Near-perfect  
309 discriminating capabilities were indicated by these scores, which ranged from 0.95 to  
310 0.98. The EfficientNetV2b0 network achieved the maximum score of 0.98. Such  
311 performance highlighted the models' capability to distinguish between the two  
312 groups with little overlap in prediction results, indicating their efficacy in utilising  
313 fine-tuned characteristics for precise glaucoma evaluation.

314 Second, the global accuracy findings showed that these models were robust and  
315 performed exceptionally well across all the fine-tuned architectures. While more  
316 complex models, like VGG16 and InceptionV3, got accuracies of 0.89,

317 EfficientNetV2b0 and ResNet50 achieved an accuracy of 0.93. The models'  
318 capacity to reliably categorise both healthy and glaucomatous samples was  
319 demonstrated by these high accuracy values, which also indicated how well they  
320 adapted to a variety of data properties. Top-tier performance was seen across the DL  
321 models in terms of sensitivity, which measured the model's capacity to identify  
322 glaucomatous cases. InceptionV3, EfficientNetV2b0, and ResNet50 achieved  
323 remarkable sensitivity values ranging from 0.86 to 0.89, demonstrating the model's  
324 ability to identify glaucomatous patients. Excellent outcomes were also shown by the  
325 F1-score, which was a harmonic mean of precision and recall for each of the five  
326 models.

327 The current study has limitations. Although the proposed models achieved high  
328 accuracy, the datasets used were limited in diversity and sample size, which may  
329 have affected the generalisability of the findings to broader populations.  
330 Furthermore, the study was based on retrospective, publicly available data without  
331 clinical validation. Future work should focus on testing the model in real-world  
332 clinical settings and improving interpretability through visualisation techniques.

333

### 334 **Conclusion**

335 The consistently high AUROC values, along with strong sensitivity and F1-scores,  
336 suggested that the models could effectively capture meaningful retinal patterns  
337 associated with glaucoma rather than simply memorising the training data. The  
338 superior performance of EfficientNetv2b0 indicated that its balanced architecture  
339 and efficient feature scaling may offer advantages over deeper but less optimised  
340 networks. The proposed model could be used for screening purposes and may help in  
341 managing human workload.

342

343

344

345 **Disclaimer:** None.

346 **Conflict of Interest:** None.

347 **Source of Funding:** None.

348

## 349 **References**

- 350 1. Sharon Kingman. Glaucoma is second leading cause of blindness globally.  
351 Bulletin of the World Health Organization, 82:887–888, 2004.
- 352 2. Harry A Quigley and Aimee T Broman. The number of people with glaucoma  
353 worldwide in 2010 and 2020. British journal of ophthalmology, 90(3):262–  
354 267.2019
- 355 3. Yih-Chung Tham, Xiang Li, Tien Y Wong, Harry A Quigley, Tin Aung, and  
356 Ching-Yu Cheng. Global prevalence of glaucoma and projections of glaucoma  
357 burden through 2040: a systematic review and meta-analysis. Ophthalmology,  
358 121(11):2081–2090, 2014.
- 359 4. Gheisari, S., Shariflou, S., Phu, J., Kennedy, J.J., Agar, A., Kalloniatis, M. et al.,  
360 2021. A combined convolutional and recurrent neural network for enhanced  
361 glaucoma detection. *Scientific reports*, 11(1), p.1945.
- 362 5. Aljohani, A. and Aburasain, R.Y., 2024. A hybrid framework for glaucoma  
363 detection through federated machine learning and deep learning models. *BMC*  
364 *Medical Informatics and Decision Making*, 24(1), p.115.
- 365 6. Jun Cheng, Jiang Liu, Yanwu Xu, Fengshou Yin, Damon Wing Kee Wong,  
366 Ngan-Meng Yan, et al. Superpixel classifica- tion based optic disc and optic cup  
367 segmentation for glaucoma screening. IEEE transactions on medical imaging,  
368 32(6):1019– 1032, 2013.
- 369 7. Saha, S., Vignarajan, J. and Frost, S., 2023. A fast and fully automated system  
370 for glaucoma detection using color fundus photographs. *Scientific*  
371 *Reports*, 13(1), p.18408.
- 372 8. Amed Mvoulana, Rostom Kachouri, and Mohamed Akil. Fully automated  
373 method for glaucoma screening using robust optic nerve head detection and  
374 unsupervised segmentation based cup-to-disc ratio computation in retinal

- 375 fundus images. *Computerized Medical Imaging and Graphics*, 77:101643,  
376 2019.
- 377 9. Sivaswamy, J., Krishnadas, S. R., Joshi, G. D., Jain, M., & Tabish, A. U.  
378 (2014). Drishti-GS: Retinal image dataset for optic nerve head (ONH)  
379 segmentation. In *IEEE 11th International Symposium on Biomedical Imaging*  
380 (ISBI), 53–56.
- 381 10. Fengshou Yin, Jiang Liu, Damon Wing Kee Wong, Ngan Meng Tan, Carol  
382 Cheung, Mani Baskaran, et al. Automated segmentation of optic disc and optic  
383 cup in fundus images for glaucoma diagnosis. In *2012 25th IEEE International*  
384 *Symposium on Computer-Based Medical Systems (CBMS)*, pages 1–6, 2012.
- 385 11. Jun Cheng, Jiang Liu, Yanwu Xu, Fengshou Yin, Damon Wing Kee Wong,  
386 Ngan-Meng Tan, et al. Superpixel classification based optic disc and optic cup  
387 segmentation for glaucoma screening. *IEEE Transactions on Medical Imaging*,  
388 32(6):1019–1032, 2013.
- 389 12. Chen, D., Ran, E.A., Tan, T.F., Ramachandran, R., Li, F., Cheung, C., et al.,  
390 2023. Applications of artificial intelligence and deep learning in glaucoma. *The*  
391 *Asia-Pacific Journal of Ophthalmology*, 12(1), pp.80-93.
- 392 13. Yann LeCun, Le'on Bottou, Yoshua Bengio, and Patrick Haffner. Gradient-  
393 based learning applied to document recognition. *Proceedings of the IEEE*,  
394 86(11):2278–2324, 2021.
- 395 14. Alex Krizhevsky, Ilya Sutskever, and Geoffrey E Hinton. Im-  
396 agenet classification with deep convolutional neural networks. *Advances in neural*  
397 *information processing systems*, 25, 2022.
- 398 15. Hongyu Chen, Yanwu Xu, Damon Wing Kee Wong, Tien Yin Wong, and  
399 Jiang Liu. Glaucoma detection based on deep con-  
400 volutional neural network. In *2015 37th Annual International Conference of the IEEE Engineering in*  
401 *Medicine and Biology Society (EMBC)*, pages 715–718, 2015.
- 402 16. Hanan S Alghamdi, Hongying Lilian Tang, Saad A Waheeb, and Tunde Peto.  
403 Automatic optic disc abnormality detection in fundus images: A deep learning

- 404 approach. In Proceedings of the ophthalmic medical image analysis  
405 international work- shop, volume 3. University of Iowa, 2016.
- 406 17. Jose´ Ignacio Orlando, Elena Prokofyeva, Mariana del Fresno, and Matthew B  
407 Blaschko. Convolutional neural network transfer for automated glaucoma  
408 identification. In 12th inter- national symposium on medical information  
409 processing and analysis, volume 10160, pages 241–250. SPIE, 2017.
- 410 18. Gopal Datt Joshi, Jayanthi Sivaswamy, and S. R. Krishnadas. Optic disk and  
411 cup segmentation from monocular color retinal images for glaucoma  
412 assessment. *IEEE Transactions on Medical Imaging*, 30(6):1102–1205, 2011.
- 413 19. F. Fumero, S. Alayon, J. L. Sanchez, J. Sigut, and M. Gonzalez-  
414 Hernandez. Rim-one: An open retinal image database for optic nerve  
415 evaluation. In 2011 24th International Symposium on Computer-Based  
416 Medical Systems (CBMS), pages 1–6, 2011.
- 417 20. Andres Diaz-Pinto, Sandra Morales, Valery Naranjo, Thomas Kohler, Jose M  
418 Mossi, and Amparo Navea. CNNs for automatic glaucoma assessment using  
419 fundus images: an extensive validation. *Biomedical engineering online*, 18:1–  
420 19, 2019.
- 421 21. Budai, A., Bock, R., Maier, A., Hornegger, J., & Michelson, G. (2013). Robust  
422 vessel segmentation in fundus images. *International Journal of Biomedical  
423 Imaging*, 2013, 154860.
- 424 22. Sokolova M, Lapalme G. A systematic analysis of performance measures for  
425 classification tasks. *Information Processing & Management*. 2009;45(4):427–  
426 437. doi: 10.1016/j.ipm.2009.03.002.
- 427 23. Pedregosa, Fabian, Gaël Varoquaux, Alexandre Gramfort, Vincent Michel,  
428 Bertrand Thirion, Olivier Grisel, Mathieu Blondel et al. "Scikit-learn: Machine  
429 learning in Python." *the Journal of machine Learning research* 12 (2011):  
430 2825-2830.
- 431 24. Harris, Charles R., K. Jarrod Millman, Stéfan J. Van Der Walt, Ralf Gommers,  
432 Pauli Virtanen, David Cournapeau, Eric Wieser et al. "Array programming with

- 433 NumPy." *nature* 585, no. 7825 (2020): 357-362.
- 434 25. Tan, M. and Le, Q., 2019, May. EfficientNet: Rethinking model scaling for  
 435 convolutional neural networks. In *International conference on machine*  
 436 *learning* (pp. 6105-6114). PMLR.
- 437 26. Chollet, F., 2017. Xception: Deep learning with depthwise separable  
 438 convolutions. In *Proceedings of the IEEE conference on computer vision and*  
 439 *pattern recognition* (pp. 1251-1258).
- 440 27. Szegedy, C., Vanhoucke, V., Ioffe, S., Shlens, J. and Wojna, Z., 2016.  
 441 Rethinking the inception architecture for computer vision. In *Proceedings of*  
 442 *the IEEE conference on computer vision and pattern recognition* (pp. 2818-  
 443 2826).
- 444 28. Simonyan, K. and Zisserman, A., 2014. Very deep convolutional networks for  
 445 large-scale image recognition. *arXiv preprint arXiv:1409.1556*.
- 446 29. He, K., Zhang, X., Ren, S. and Sun, J., 2016. Deep residual learning for image  
 447 recognition. In *Proceedings of the IEEE conference on computer vision and*  
 448 *pattern recognition* (pp. 770-778).

449 -----

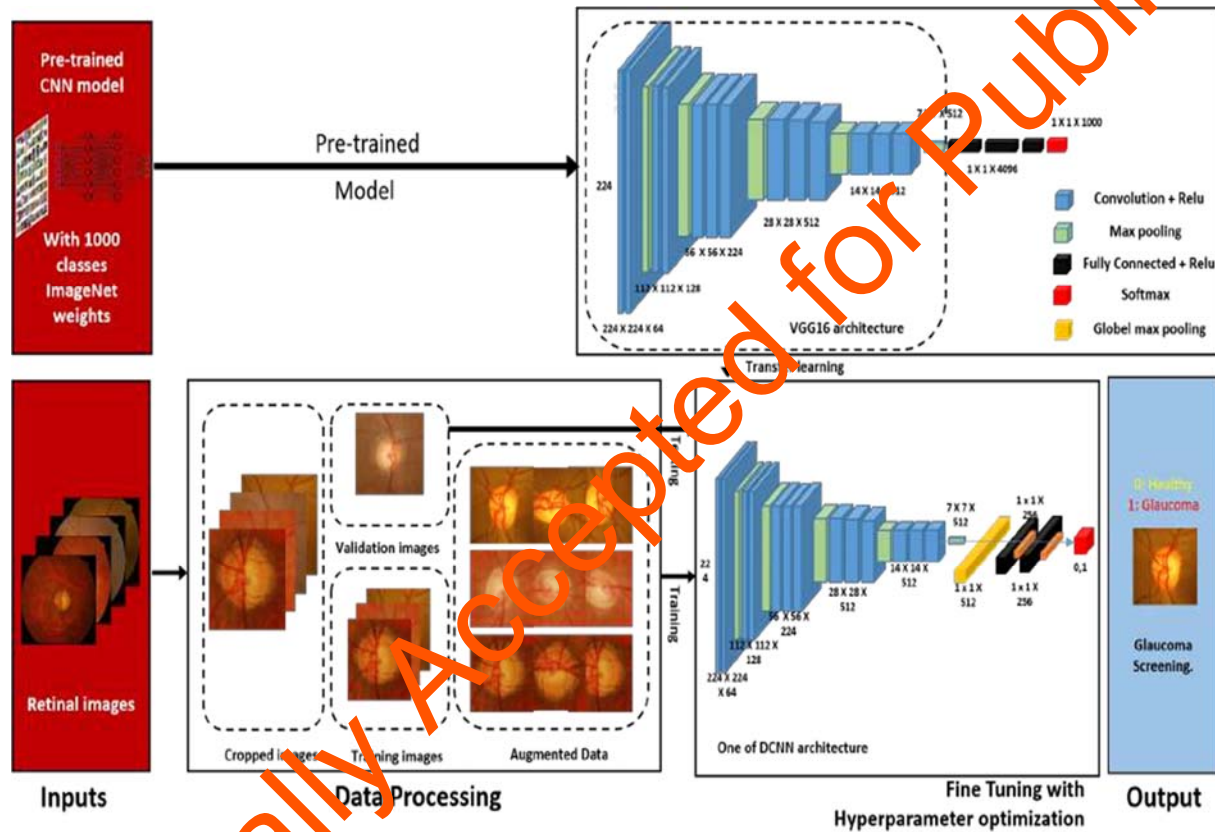
451  
 452 **Table 1: Comparison of retinal image datasets for glaucoma screening and**  
 453 **performance analysis of the proposed method with earlier studies on glaucoma**  
 454 **detection.**

Dataset	Healthy	Glaucomatous			Total
DRISHTI-GS [09]	31	70			101
RIM-ONE [19]	261	194			455
HRF [21]	18	27			45
Sjchoi86 HRF [21].	300	101			301
ACRIMA [20]	309	396			705
Models	AUC	Accuracy	Precision	Recall	F1-Score
VGG19 [19]	0.96	0.90	0.88	0.92	0.91
InceptionV3 [19]	0.96	0.90	0.86	0.92	0.90
Inception [19]	0.96	0.89	0.78	0.93	0.90
VGG16 [19]	0.96	0.89	0.84	0.90	0.90
ResNet50 [19]	0.96	0.89	0.89	0.93	0.90
EfficientNetV2B0 (ours)	0.98	0.93	0.88	0.97	0.93
InceptionV3 (ours)	0.96	0.89	0.86	0.92	0.89
Xception (ours)	0.95	0.85	0.78	0.93	0.85
VGG16 (ours)	0.96	0.89	0.84	0.93	0.89

ResNet50 (ours)	0.98	0.93	0.89	0.97	0.93
-----------------	------	------	------	------	------

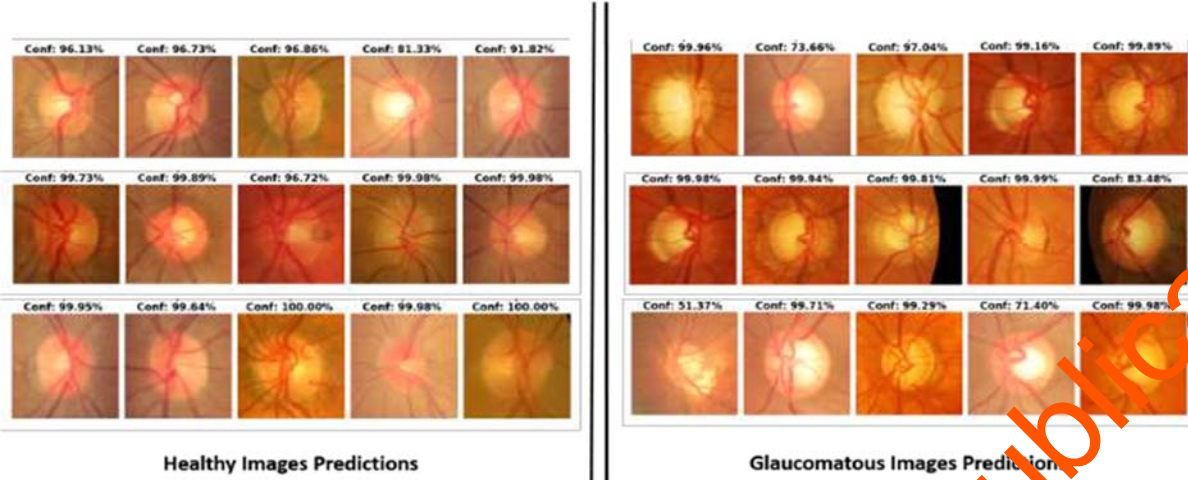
455 **Abbreviations:** *DRISHTI-GS*, retinal fundus image dataset for optic nerve head segmentation and  
 456 glaucoma assessment; *RIM-ONE*, Retinal Images for Optic Nerve Evaluation; *HRF*, High-Resolution  
 457 Fundus; *Sjchoi86-HRF*, retinal fundus image dataset derived from Sjchoi86 and HRF images;  
 458 *ACRIMA*, retinal fundus image dataset/project used for glaucoma classification; *AUC*, area under the  
 459 receiver operating characteristic curve; *VGG*, Visual Geometry Group; *ResNet*, Residual Network;  
 460 *EfficientNetV2B0*, EfficientNet Version 2 B0 variant; *F1-score*, harmonic mean of precision and  
 461 recall.

462  
 463  
 464



465  
 466 **Figure 1: “Overall workflow of the proposed glaucoma classification**  
 467 **method, including pre-processing, model training (VGG16), and final**  
 468 **classification”.**

469  
 470  
 471



472

473

474

475

476

477

478

479

480

481

482

483

484

485

**Figure 2: Examples of correctly classified retinal images, using EfficientNetV2-B0 model, along with the prediction score on the ground-truth class.**

Submission completed	18-06-2025
1st Revision received	24-10-2025
Last Revision received	29-05-2026
Acceptance	30-05-2026

**AUTHORS' CONTRIBUTIONS:**

**NR & ZS:** Drafting, data acquisition, analysis and interpretation.

**FS:** Concept, drafting and revision.

**SFB:** Data acquisition, analysis and interpretation.

**MA & FA:** Concept, design, revision and final approval.

Provisionally Accepted for Publication